AIAA JOURNAL
Vol. 33, No. 10, October 1995

Matrix Dissipation for Central Difference Schemes with Combustion

P. Gerlinger,* J. Algermissen,† and D. Brüggemann†
University of Stuttgart, 70550 Stuttgart, Germany

The effect of artificial viscosity is investigated for problems related to supersonic combustion. An implicit lower-upper symmetric Gauss–Seidel finite volume method is employed for solving the full, compressible, two-dimensional averaged Navier–Stokes and species transport equations. For the right-hand side discretization central differences are used. Therefore some kind of artificial viscosity is necessary to reduce oscillations near shock waves and to enable convergence to machine accuracy. In comparison to the standard second- and fourth-order scalar dissipation a matrix dissipation reduces the amount of artificial viscosity by scaling each equation individually. For the necessary absolute flux Jacobian matrix a new decomposition is presented keeping the additional cost moderate. With an appropriate sensor the scheme also gets total variation diminishing properties. Calculations using different dissipation models are presented and advantages using a matrix dissipation are shown.

Introduction

CENTRAL difference schemes are often applied to solve the Euler or Navier–Stokes equations.[1] This is done even for hypersonic flows in conjunction with multigrid acceleration techniques.[2–4] In these cases the added artificial viscosity plays an important role in stabilizing the numerical scheme to reach a steady state. A matrix dissipation allows the reduction of the amount of added artificial viscosity. This feature is also important for damping the turbulence transport equations, especially if a low-Reynolds-number model is used. The strong gradients in the near-wall regions often cause large values of artificial viscosity that can contaminate the physical dissipation. However, the matrix dissipation process is normally paid by a strong increase in operation counts. Especially for cases including combustion with typically a large number of different species conservation equations, an efficient and economic way to perform the dissipation process is crucial.

Governing Equations and Numerical Scheme

The two-dimensional, averaged Navier–Stokes and species transport equations for a chemically reacting gas of N_k different species are given by

$$\frac{\partial \boldsymbol{Q}}{\partial t} + \frac{\partial (\boldsymbol{F} - \boldsymbol{F}_v)}{\partial x} + \frac{\partial (\boldsymbol{G} - \boldsymbol{G}_v)}{\partial y} = \boldsymbol{S} \tag{1}$$

where

$$\boldsymbol{Q} = [\rho, \rho u, \rho v, \rho E, \rho Y_k]^t \tag{2}$$

$$\boldsymbol{F} = \begin{bmatrix} \rho u \\ \rho u^2 + p \\ \rho uv \\ u(\rho E + p) \\ \rho u Y_k \end{bmatrix}, \qquad \boldsymbol{F}_v = \begin{bmatrix} 0 \\ \tau_{xx} \\ \tau_{xy} \\ u\tau_{xx} + v\tau_{xy} - q_x \\ -\rho \tilde{u}_k Y_k \end{bmatrix} \tag{3}$$

$$\boldsymbol{G} = \begin{bmatrix} \rho v \\ \rho uv \\ \rho v^2 + p \\ v(\rho E + p) \\ \rho v Y_k \end{bmatrix}, \qquad \boldsymbol{G}_v = \begin{bmatrix} 0 \\ \tau_{xy} \\ \tau_{yy} \\ u\tau_{xy} + v\tau_{yy} - q_y \\ -\rho \tilde{v}_k Y_k \end{bmatrix} \tag{4}$$

$$\boldsymbol{S} = [0, 0, 0, 0, W_k]^t \tag{5}$$

for $k = 1, 2, \ldots, N_k - 1$. In this set of equations the physical variables are the density ρ, the velocity components u and v in the x and y directions, the pressure p, the temperature T, the total specific energy E, and the species mass fractions Y_k. The diffusion velocities are $\tilde{u}_k$ and $\tilde{v}_k$, and the source term for species k due to chemical reactions is W_k. The governing equations are closed by a two-equation q-ω low-Reynolds-number turbulence model.[5,6] The combustion process in chemical nonequilibrium is modeled by a 9-species, 20-step finite rate chemistry model[7] and is implicitly coupled with the fluid motion.

For solving the governing equations as well as the turbulence transport equations (in a decoupled way) an implicit lower-upper symmetric Gauss–Seidel (LU-SGS) method is used.[1,8] If source terms exist, there are different possibilities of approximate factorization that result in LU schemes. In this paper the factorization of Shuen[9] is used. The low-Reynolds-number turbulence closure needs very fine grids in the near-wall regions, making it advantageous to include viscous Jacobians in the implicit operator. This is done in a simplified form, based on the thin-layer Navier–Stokes equations.[9] The LU scheme results in block diagonal operators and is fully vectorizable also in the implicit part.

Artificial Viscosity

Because central differences are used for the spatial derivatives of the right-hand side (RHS), it is necessary to add some kind of artificial viscosity. Near shock waves second differences are added to avoid spurious oscillations, whereas fourth-order differences are added in the smooth regions of the flowfield to suppress "odd-even oscillations" and enable convergence to a steady state. The added artificial dissipation may be expressed in curvilinear ξ and η coordinates by

$$\boldsymbol{AD}_{i,j} = \left(D_\xi^2 + D_\eta^2 - D_\xi^4 - D_\eta^4\right)\boldsymbol{Q}_{i,j} \tag{6}$$

where D^2 and D^4 are spatial difference operators

$$\begin{aligned} D_\xi^2 \boldsymbol{Q} &= \nabla_\xi \left[\left(|A|_{i+\frac{1}{2},j} \epsilon^{(2)}_{i+\frac{1}{2},j} \right) \Delta_\xi \right] \boldsymbol{Q}_{i,j} \\ D_\xi^4 \boldsymbol{Q} &= \nabla_\xi \left[\left(|A|_{i+\frac{1}{2},j} \epsilon^{(4)}_{i+\frac{1}{2},j} \right) \Delta_\xi \nabla_\xi \Delta_\xi \right] \boldsymbol{Q}_{i,j} \end{aligned} \tag{7}$$

Received May 5, 1994; presented as Paper 94-3181 at the AIAA/ASME/SAE/ASEE 30th Joint Propulsion Conference, Indianapolis, IN, June 27–29, 1994; revision received March 27, 1995; accepted for publication April 4, 1995.

*Research Scientist, Department of Aerospace Engineering, Pfaffenwaldring 31. Member AIAA.
†Professor, Department of Aerospace Engineering, Pfaffenwaldring 31.

and ∇_ξ and Δ_ξ are backward and forward difference operators, respectively,

$$\begin{aligned}\Delta_\xi \boldsymbol{Q}_{i,j} &= \boldsymbol{Q}_{i+1,j} - \boldsymbol{Q}_{i,j} \\ \nabla_\xi \boldsymbol{Q}_{i,j} &= \boldsymbol{Q}_{i,j} - \boldsymbol{Q}_{i-1,j}\end{aligned} \tag{8}$$

If in Eq. (7) the spectral radius $\rho(\boldsymbol{A}_{i+1/2,j})$ instead of the absolute flux Jacobian $|\boldsymbol{A}|_{i+1/2,j}$ is used, we get the standard scalar second- and fourth-order dissipation model that was first introduced by Jameson et al.[10] This model is called scalar because every equation is scaled with the same value. If $|\boldsymbol{A}|_{i+1/2,j}$ is used, we obtain the matrix dissipation introduced by Turkel,[11] Turkel and Vatsa,[13] and Swanson and Turkel.[2] Now each equation is scaled by an individual value reducing the amount of added artificial viscosity. The coefficients $\epsilon^{(2)}$ and $\epsilon^{(4)}$, which depend on the pressure gradient parameter ν, are used to locate shock waves within the flowfield and are defined as

$$\nu_{i,j} = \frac{|p_{i+1,j} - 2p_{i,j} + p_{i-1,j}|}{[(1-\chi)(|p_{i+1,j}-p_{i,j}|+|p_{i,j}-p_{i-1,j}|)+\chi(p_{i+1,j}+2p_{i,j}+p_{i-1,j})]} \tag{9}$$

$$\epsilon^{(2)}_{i+\frac{1}{2},j} = \kappa^{(2)} \max(\nu_{i,j}, \nu_{i+1,j}) \tag{10}$$

$$\epsilon^{(4)}_{i+\frac{1}{2},j} = \kappa^{(4)} \max\left(0, 1 - 2\nu_{i+\frac{1}{2},j}\right) \tag{11}$$

Swanson and Turkel[2] could show for a scalar equation that with a constant value of $\kappa^{(2)} = 0.5$ the scheme is first-order upwind near shocks. The remaining free parameter is $\kappa^{(4)}$, which is responsible for the amount of artificial dissipation in the smooth flow regions. The fourth-order dissipation is cut off in the vicinity of shock waves for $\nu_{i+1/2,j} \geq 1/2$. For $\chi = 1$ the original switch is obtained,[10] which is not total variation diminishing (TVD), whereas for $\chi \approx 0$ the scheme satisfies the TVD property[2] but is in general too dissipative for the use over a wide range of flow problems. However, with χ there is now the possibility to blend over between both switches. An optimal value depends upon the strength of the shocks to be resolved. For computing transonic flows Turkel[11] used $\chi \approx 0$, whereas for hypersonic flows Vatsa et al.[3] used $\chi = 0.5$.

The matrix $|\boldsymbol{A}|_{i+1/2,j}$ has to be formed at the cell interface, which is done by a simple averaging of the solution vector $\boldsymbol{Q}$ instead of a Roe averaging.[11] The absolute flux Jacobian $|\boldsymbol{A}|_{i+1/2,j}$ is defined by

$$\begin{aligned}\boldsymbol{A} &= \boldsymbol{T}\boldsymbol{\Lambda}\boldsymbol{T}^{-1} \\ |\boldsymbol{A}| &= \boldsymbol{T}|\boldsymbol{\Lambda}|\boldsymbol{T}^{-1}\end{aligned} \tag{12}$$

where the diagonal matrix $\boldsymbol{\Lambda}$ contains the three different eigenvalues of $\boldsymbol{A}$ as elements

$$\boldsymbol{\Lambda} = \mathrm{diag}[\lambda_1, \lambda_2, \lambda_3, \lambda_3, \ldots, \lambda_3] \tag{13}$$

and the columns of the transformation matrix $\boldsymbol{T}$ are the right eigenvectors of $\boldsymbol{A}$. For curvilinear coordinates the metrics of the concerned cell interface are included in the eigenvalues

$$\begin{aligned}\lambda_1 &= (u_n + a)\,\Delta s & \lambda_3 &= u_n\,\Delta s \\ \lambda_2 &= (u_n - a)\,\Delta s & u_n &= c_1 u + c_2 v \\ c_1 &= \frac{\Delta y}{\Delta s} & c_2 &= -\frac{\Delta x}{\Delta s}\end{aligned} \tag{14}$$

where a is the speed of sound, Δs is the cell interface length, and Δx and Δy are the parts of this length in x and y directions. These differences have to be calculated for every cell in counterclockwise fashion. For a multicomponent gas with combustion the pressure derivatives with respect to the variable vector $\boldsymbol{Q}$ are needed to form the Jacobian $\boldsymbol{A}$. Because only $N_k - 1$ different species are independent variables, we get for the pressure as a function of the variable vector $\boldsymbol{Q}$

$$p = R_m T\left[\frac{\rho}{M_{N_k}} + \sum_{k=1}^{N_k-1} \rho Y_k\left(\frac{1}{M_k} - \frac{1}{M_{N_k}}\right)\right] \tag{15}$$

where M_k is the molecular weight of species k and R_m is the universal gas constant. Using the specific internal energy $e = E - 1/2(u^2+v^2) - k$ where the turbulent kinetic energy k is included, the necessary pressure derivatives may be formed by chain rule.[13] For all following derivatives the remaining conservative variables are treated as constant:

$$\frac{\partial p}{\partial \rho} = \frac{R_m T}{M_{N_k}} + \frac{R_m}{M c_v}\left[-E + u^2 + v^2 + \sum_{k=1}^{N_k-1} Y_k\left(e_k - e_{N_k-1}\right)\right] \tag{16}$$

$$\frac{\partial p}{\partial(\rho u)} = -\frac{R_m u}{M c_v} \tag{17}$$

$$\frac{\partial p}{\partial(\rho E)} = \frac{R_m}{M c_v} \tag{18}$$

$$\frac{\partial p}{\partial(\rho Y_i)} = R_m T\left(\frac{1}{M_i} - \frac{1}{M_{N_k}}\right) - \frac{R_m}{M c_v}\left(e_i - e_{N_k}\right) \tag{19}$$

The calculation of the absolute Jacobian $|\boldsymbol{A}|$ and the subsequent matrix vector multiplications of Eq. (7) would strongly increase the computational cost for the matrix dissipation. Turkel[11] presented for airflow a decomposition of the absolute Jacobian that simplifies this procedure. For the more complicated absolute Jacobian of a chemical nonequilibrium gas we could also find such a decomposition:

$$|\boldsymbol{A}| = \left[\frac{-1}{a^2}\cdot \boldsymbol{A}_1 + \boldsymbol{A}_2\right]\cdot|\lambda_3| + \frac{1}{2a^2}[\boldsymbol{A}_3\cdot|\lambda_1| + \boldsymbol{A}_4\cdot|\lambda_2|] \tag{20}$$

The matrix $|\boldsymbol{A}|$ is expressed now in a manner in which the matrices $\boldsymbol{A}_1, \boldsymbol{A}_3$, and $\boldsymbol{A}_4$ are formed in such a way that each lower row of these matrices is a scalar times the first row. Therefore they may be expressed by the following products of vectors:

$$\boldsymbol{A}_1 = \boldsymbol{R}_1^t \boldsymbol{R}_2 \qquad \boldsymbol{A}_3 = \boldsymbol{R}_3^t \boldsymbol{R}_4 \qquad \boldsymbol{A}_4 = \boldsymbol{R}_5^t\, \boldsymbol{R}_6 \tag{21}$$

where

$$\boldsymbol{R}_1 = \left\{1, u, v, H - \frac{a^2}{[\partial p/\partial(\rho E)]}, Y_1, \ldots, Y_{N_k-1}\right\} \tag{22}$$

$$\boldsymbol{R}_2 = \left\{\frac{\partial p}{\partial \rho} - a^2, \frac{\partial p}{\partial(\rho u)}, \frac{\partial p}{\partial(\rho v)}, \frac{\partial p}{\partial(\rho E)}, \frac{\partial p}{\partial(\rho Y_1)}, \ldots, \frac{\partial p}{\partial\left(\rho Y_{N_k-1}\right)}\right\} \tag{23}$$

$$\boldsymbol{R}_3 = \left\{1, u + c_1 a, v + c_2 a, H + a u_n, Y_1, \ldots, Y_{N_k-1}\right\} \tag{24}$$

$$\boldsymbol{R}_4 = \left\{\frac{\partial p}{\partial \rho} - a u_n,\ c_1 a + \frac{\partial p}{\partial(\rho u)}, c_2 a + \frac{\partial p}{\partial(\rho v)}, \frac{\partial p}{\partial(\rho E)}, \frac{\partial p}{\partial(\rho Y_1)}, \ldots, \frac{\partial p}{\partial\left(\rho Y_{N_k-1}\right)}\right\} \tag{25}$$

$$\boldsymbol{R}_5 = \left\{1, u - c_1 a, v - c_2 a, H - a u_n, Y_1, \ldots, Y_{N_k-1}\right\} \tag{26}$$

$$\boldsymbol{R}_6 = \left\{\frac{\partial p}{\partial \rho} + a u_n, -c_1 a + \frac{\partial p}{\partial(\rho u)}, -c_2 a + \frac{\partial p}{\partial(\rho v)}, \frac{\partial p}{\partial(\rho E)}, \frac{\partial p}{\partial(\rho Y_1)}, \ldots, \frac{\partial p}{\partial\left(\rho Y_{N_k-1}\right)}\right\} \tag{27}$$

and matrix $\boldsymbol{A}_2$ is given in Eq. (28)

$$A_2 = \begin{bmatrix} 0 & 0 & 0 & 0 & 0 & \cdots & 0 \\ -c_2(c_2u - c_1v) & c_2^2 & -c_2c_1 & 0 & 0 & \cdots & 0 \\ c_1(c_2u - c_1v) & -c_1c_2 & c_1^2 & 0 & 0 & \cdots & 0 \\ -(c_2u - c_1v)^2 + F_1 & c_2(c_2u - c_1v) & -c_1(c_2u - c_1v) & 0 & -\dfrac{\partial p/\partial(\rho Y_1)}{\partial p/\partial(\rho E)} & \cdots & -\dfrac{\partial p/\partial\left(\rho Y_{N_k-1}\right)}{\partial p/\partial(\rho E)} \\ -Y_1 & 0 & 0 & 0 & 1 & \cdots & 0 \\ \cdots & \cdots & \cdots & \cdots & \cdots & \cdots & \cdots \\ -Y_{N_k-1} & 0 & 0 & 0 & 0 & \cdots & 1 \end{bmatrix} \tag{28}$$

where

$$F_1 = \frac{1}{[\partial p/\partial(\rho E)]} \sum_{k=1}^{N_k-1} \frac{\partial p}{\partial(\rho Y_k)} Y_k \tag{29}$$

Because A_2 is a sparse matrix, the lack of a decomposition is not a serious problem. Treating the term F_1 separately, the 3 · 3 submatrix (formed by the rows 2–4 and the columns 1–3) again reveals the favorable property that the lower rows are proportional to the first row. The remaining part of row 4 is the same part of row 1 in A_1 times a scalar. Instead of calculating $|A_{i+1/2,j}|$ and multiplying with a vector, we directly multiply row and column vectors by taking advantage of the special form of $|A|$ in Eq. (20). This procedure for the first row and the scalar multiplications for all others is very efficient, especially for chemically reacting flows with numerous species conservation equations.

In practice we have to avoid individual eigenvalues approaching zero because this would result in zero artificial viscosity and could cause numerical instabilities or nonphysical solutions. Therefore limited eigenvalues $\tilde{\lambda}_i$ are used in Eq. (20) instead of the true ones:

$$|\tilde{\Lambda}| = \text{diag}[|\tilde{\lambda}_i|] = \text{diag}[\max(t_i \rho(A), |\lambda_i|)] \tag{30}$$

With $t_i = 1$ we obtain a scalar dissipation. In our calculations $t_i = 0.2$ is used for both linear and nonlinear eigenvalues. The choice of these limiters will also affect the occurence of spurious oscillations and the shock resolution.[12] It is also possible and sometimes advantageous[14] to use different values for the linear and nonlinear eigenvalues or for the different coordinate directions (streamwise or normal to solid walls).

If low-Reynolds-number turbulence models are employed, the near-wall regions have to be resolved very accurately, resulting in highly stretched grids. In these regions an isotropic scaling can produce too much numerical dissipation.[15] Therefore the limited eigenvalues are modified by

$$\hat{\lambda}_\xi = \tilde{\lambda}_\xi \left[1 + \left(\frac{\tilde{\lambda}_\eta}{\tilde{\lambda}_\xi}\right)^a\right] \tag{31}$$

to produce an anisotropic dissipation[2,15,16] where a is usually taken to be 1/2.

In some cases[17] we found it advantageous to use a further modification if a low-Reynolds-number turbulence model is employed. In the near-wall regions there may be very strong gradients in some flow variables. In this case the second- and fourth-order derivatives can be quite large, leading often to large, nonphysical values of artificial viscosity.[14] To reduce the ratio between numerical and physical smoothing Eq. (31) may be additionally multiplied with $t_c = \sqrt{(u^2 + v^2)}/w_{\text{ref}}$, because in low-speed regions the natural dissipation is already sufficient to stabilize the numerical scheme. Kunz and Lakshminarayana[16] used t_c^2 as a multiplicator, but in combination with the matrix dissipation this led in some cases to numerical instabilities.

The dissipation for the turbulence transport equations is treated in the same manner as for the mean flow equations. If the turbulence transport equations are solved in a decoupled way from the fluid motion, only diagonal Jacobians are obtained and no matrix decomposition is necessary. If the turbulence model is treated fully coupled, the decomposition of Eq. (20) can be used. Because the pressure is independent of q and ω, the pressure derivatives with respect to these turbulent variables are zero. Thus only two additional lines and columns have to be added within the matrices A_1–A_4. These lines are identical to those of the species conservation equations if Y_i is replaced by q or ω.

Results and Discussion

We consider two channel flow problems with premixed and nonpremixed supersonic combustion. The main purpose of this paper is to investigate the influence of the described kinds of artificial dissipation. This is done in the first test case. The second one is a comparison with the experiment of Burrows and Kurkov,[18] which is dominated by turbulent diffusion.

Premixed Combustion

To investigate different dissipation models, combustion of a premixed hydrogen–air supersonic flow in a ramped duct is considered. The geometry and inflow conditions are illustrated in Fig. 1. Hydrogen and air are mixed with a fuel equivalence ratio of $\Phi = 1$ at the channel entrance. The calculation is performed with a one block grid consisting of 180 × 110 volumes. The temperature is increased significantly above the ignition threshold by the viscous layer along the wall and the shock that is induced by the ramp at the lower wall. This case is chosen because results of other researchers[1,19–21] are available, among which is the solution of Yee and Shinn,[20,21] who used a TVD shock-capturing scheme. Figures 2–4 show pressure profiles in different planes away from the lower wall. In every figure results of five calculations are presented that are obtained using different kinds of artificial dissipation. In general the amount of artificial viscosity is reduced by the matrix dissipation and increased by the TVD sensor [small values of χ in Eq. (9)]. Therefore the calculation with scalar dissipation employing the TVD sensor ($\chi = 0.00001$) adds the greatest amount of artificial viscosity. The other extreme is the matrix dissipation with the standard sensor ($\chi = 1$) that adds the smallest amount. The two calculations without

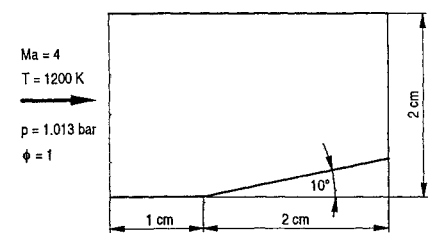

Fig. 1 Geometry and inflow conditions.

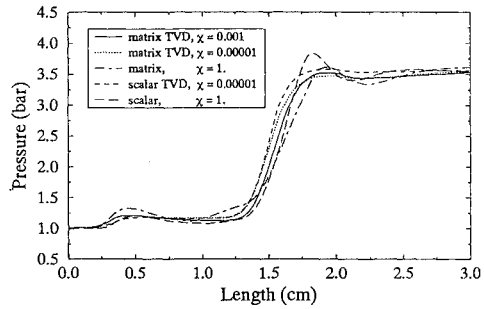

Fig. 2 Pressure distributions at the plane y = 0.13 cm away from the lower wall.

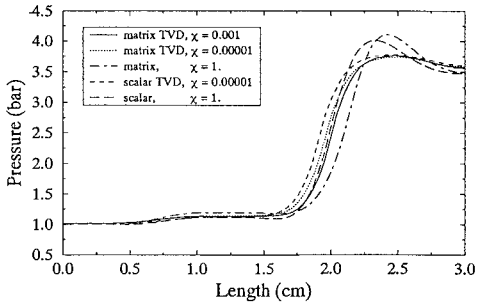

Fig. 3 Pressure distributions at the plane $y = 0.29$ cm away from the lower wall.

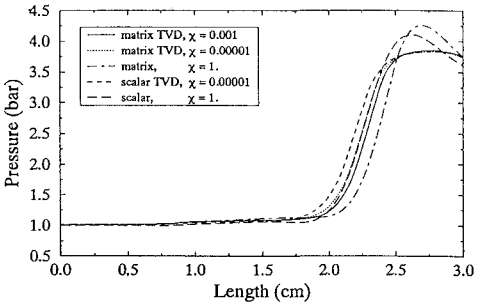

Fig. 4 Pressure distributions at the plane $y = 0.42$ cm away from the lower wall.

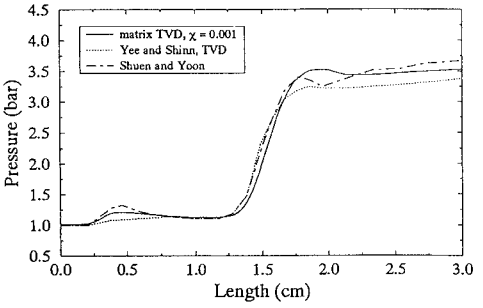

Fig. 5 Pressure distributions at the plane $y = 0.13$ cm away from the lower wall.

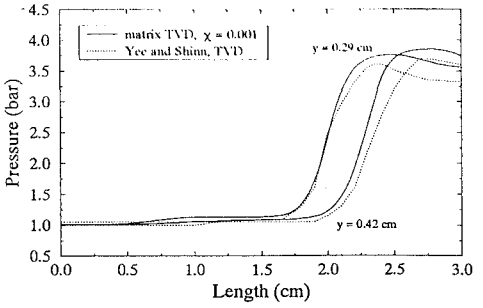

Fig. 6 Pressure distributions at the plane $y = 0.29$ and $y = 0.42$ cm away from the lower wall.

the TVD sensor show strong overshoots in pressure that increase with growing distance from the wall. In general these overshoots are still increased if the amount of artificial viscosity is reduced by the matrix dissipation. Improvement is achieved using small values of χ to get TVD properties. The overshoots disappear but on the other side the shocks get more smeared. Therefore the value for χ has to be chosen very carefully. In our investigations we worked with constant values, but it would be desirable to determine this value depending on the strength of the shocks to be resolved. In addition it is important to employ the described matrix dissipation if the TVD sensor is used. Figure 3 shows clearly that the smearing of the shock is reduced by the matrix dissipation in comparison with the scalar one. In Figs. 5 and 6 results are compared with

Table 1 Flow conditions for Burrows–Kurkov combustion experiment

	Hydrogen jet	Air mainstream
p, bar	1	1
T, K	254	1270
Ma	1	2.44
Y_{H_2}	1	0
Y_{N_2}	0	0.486
Y_{O_2}	0	0.258
Y_{H_2O}	0	0.256

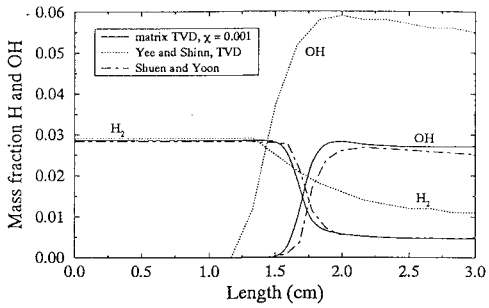

Fig. 7 Mass fraction profiles of H_2 and OH for the plane $y = 0.13$ cm away from the lower wall.

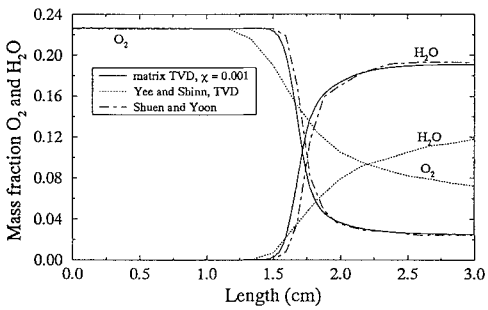

Fig. 8 Mass fraction profiles of O_2 and H_2O for the plane y = 0.13 cm away from the lower wall.

those of other researchers. Shuen and Yoon used a non-TVD central difference scheme and a detailed 8-species, 14-step chemistry model. From this calculation only a less critical near-wall profile is available. The overall agreement with this calculation is quite good, especially the combustion dominated levels of pressure and species mass fractions behind the shock wave. The shock resolution of the matrix TVD dissipation is comparable to those obtained by the shock-capturing TVD scheme of Yee and Shinn. However, a much finer grid was used in our calculation to get a grid-independent solution. The simplified five-species, two-step global combustion model of Yee and Shinn seems to be responsible for the difference in pressure level behind the shock wave. Still stronger disparities occur in the composition profiles, given in Figs. 7 and 8. However, our results agree very well with those of Shuen and Yoon, making the different chemistry models responsible for these differences.

Burrows–Kurkov Combustion Experiment

Burrows and Kurkov[18] conducted a supersonic hydrogen wall jet experiment including combustion. The geometry of the test section that is identical to the computed field is given in Fig. 9. The used computational grid consisted of 2 blocks with 99×57 and 119×75 volumes. The boundary line between the two blocks is the nearly horizontal line plotted in Fig. 11 that separates the lower and the upper channel part. The grid resolves the lip above the injector, having a strong influence on the resulting flow pattern. The high temperature gas stream for this experiment was produced by precombustion being performed in such a way that the gas, entering the test section, contained a definite fraction of oxygen and no hydrogen. The conditions for the vitiated airstream and the sonically injected hydrogen appear in Table 1. The calculation starts 2 cm upstream of the wall

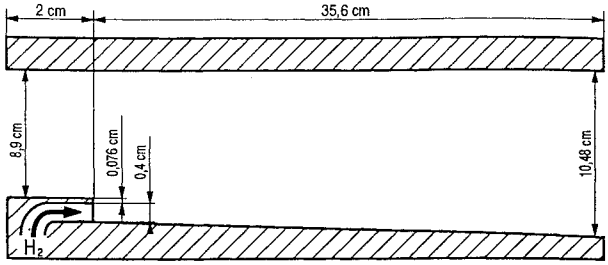

Fig. 9 Geometry for the Burrows–Kurkov experiment.

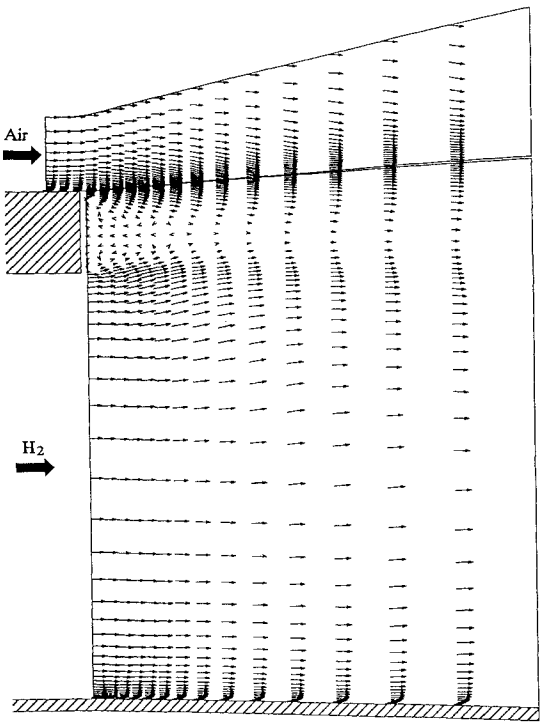

Fig. 10 Velocity vectors near the injector.

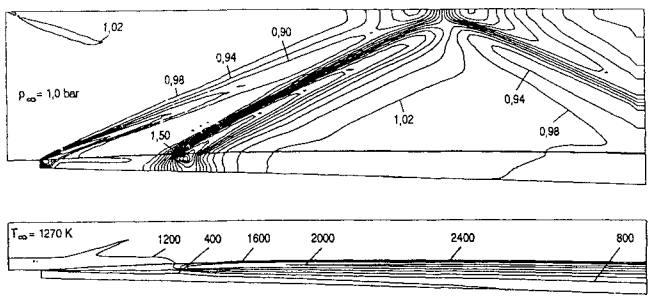

Fig. 11 Calculated pressure and temperature contours using the matrix dissipation model.

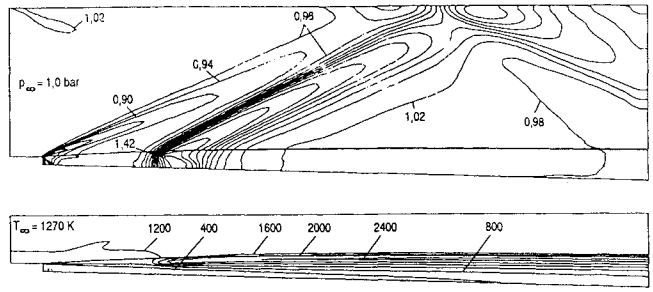

Fig. 12 Calculated pressure and temperature contours the TVD matrix dissipation model.

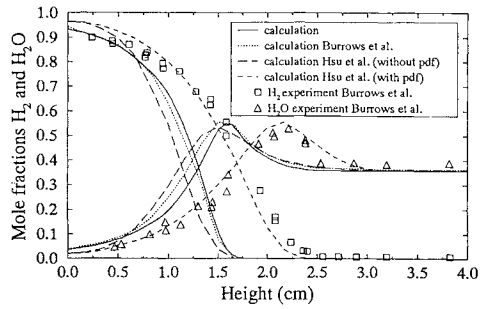

Fig. 13 Mole fraction profiles for H_2 and H_2O at the location x = 35.6 cm.

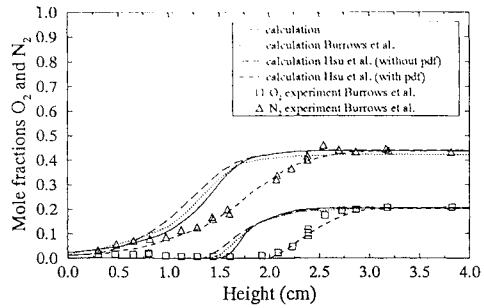

Fig. 14 Mole fraction profiles for O_2 and N_2 at the location x = 35.6 cm.

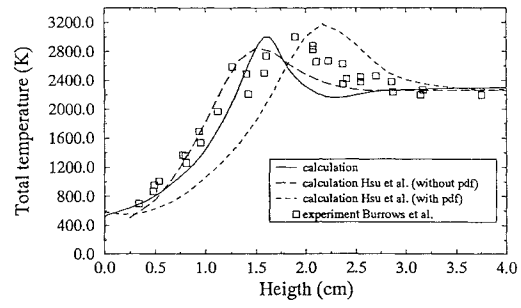

Fig. 15 Total temperature profiles for x = 35.6 cm.

step where fully turbulent inlet profiles for velocity, temperature, and turbulence variables are assumed. The boundary-layer thickness of about 1.2 cm is known from experiment. A velocity vector plot of the region near the injector is shown in Fig. 10. At the lower and upper corners of the injector lip expansion fans are formed that are followed by weak shock waves. This is due to the change in flow direction and may also be observed in the pressure contours given in Figs. 11 and 12 that are calculated with different matrix dissipation models. For the first calculation the original sensor ($\chi = 1$) is used, whereas for the second one a TVD sensor, ($\chi = 0.00001$) is employed. The oscillations in front and behind of the shocks are reduced by the TVD sensor, but again the more dissipative behavior results in a stronger smearing. Figures 11 and 12 additionally show the temperature contours for the lower channel part where combustion takes place. After a definite ignition length a strong rise in temperature may be observed. The ignition induces a strong shock wave that is visible in the pressure distributions. In experiment, ignition was determined from photographs of the radiation[18] to take place about 16 cm downstream of the injector. The calculated ignition length is influenced by the used dissipation model. If the more dissipative TVD sensor is applied, ignition occurs about 7 cm downstream of the injector, whereas it takes 8.2 cm in the case of matrix dissipation without the TVD sensor. However, there was no visible difference within the composition profiles at the end of the test section. Figures 13 and 14 show mole fraction profiles from experiment and calculations of different researchers for the cross section 35.6 cm downstream of the injector. Hsu et al.[22] used a probability density function (PDF) method to account for turbulence chemistry interactions. With exception of this calculation all profiles seem to be shifted towards the wall in comparison with the experiment. The better description of physics by the use of PDFs

seems to be responsible for the improvements in the results of Hsu et al.[22] However, in this calculation global chemistry with partial equilibrium was employed, and the lip thickness at the injector was neglected. Therefore ignition already occurred in the plane of the injector exit and no shock system was obtained. Figure 15 shows the total temperature distributions. Again our results compare quite well with the experiment up to a height of 1.5 cm, whereas there are differences in regions more distant from the wall. The peak total temperature agrees very well with the experimental value.

Conclusions

Different kinds of second- and fourth-order artificial viscosity have been investigated. As shown, the amount of artificial viscosity is reduced by the use of a matrix instead of a scalar dissipation model. The numerical effort for this procedure is significantly reduced by the presented decomposition of the necessary absolute flux Jacobian. Oscillations in front and behind of shock waves are reduced using a TVD sensor. Because this sensor is more dissipative than the original one it has to be handled very carefully and should be used in combination with the matrix dissipation.

Acknowledgment

We wish to thank the Deutsche Forschungsgemeinschaft (DFG) for the financial support of this work within the SFB 259 at the University of Stuttgart.

References

[1]Shuen, J. S., and Yoon, S., "Numerical Study of Chemically Reacting Flows Using an LU Scheme," AIAA Paper 88-0436, Jan. 1988.

[2]Swanson, R. C., and Turkel, E.,"On Central Difference and Upwind Schemes," NASA CR 182061, June 1990.

[3]Vatsa, V. N., Turkel, E., and Abolhassani, J. S., "Extension of Multigrid Methodology to Supersonic/Hypersonic 3-D Viscous Fows," NASA CR 187612, Aug. 1991.

[4]Decker, N. H., and Turkel, E., "Multigrid for Hypersonic Inviscid Flows," NASA ICASE Rept. 90-54, Aug. 1990.

[5]Coakley, T. J., and Huang, P. G., "Turbulence Modeling for High Speed Flows," AIAA Paper 92-0436, Jan. 1992.

[6]Gerlinger, P., and Algermissen, J.,"Numerical Calculation of Supersonic Combustion Problems Using an Implicit LU-SGS Scheme and k-ϵ/q-ω Turbulence Closure," AIAA Paper 93-5021, Dec. 1993.

[7]Jachimowski, C. J., "An Analytical Study of the Hydrogen-Air Reaction Mechanism with Application to Scramjet Combustion," NASA TP 2791, Feb. 1988.

[8]Yoon, S., and Jameson, A., "An LU-SSOR Scheme for the Euler and Navier–Stokes Equations," AIAA Paper 87-0600, Jan. 1987.

[9]Shuen, J. S., "Upwind Differencing and LU Factorization for Chemical Non-Equilibrium Navier–Stokes Equations," *Journal of Computational Physics*, Vol. 99, 1992, pp. 233–250.

[10]Jameson, A., Schmidt, W., and Turkel, E., "Numerical Solution of the Euler Equations by Finite Volume Methods Using Runge–Kutta Time Stepping Schemes," AIAA Paper 81-1259, June 1981.

[11]Turkel, E., "Improving the Accuracy of Central Difference Schemes," *11th International Conference on Numerical Methods in Fluid Dynamics*, Vol. 323, Lecture Note in Physics, Springer–Verlag, New York, 1988, pp. 586–591.

[12]Turkel, E., and Vatsa, V. N., "Effect of Artificial Viscosity on Three-Dimensional Flow Solutions," *AIAA Journal*, Vol. 32, No. 1, 1994, pp. 39–45.

[13]Shuen, J. S., Liou, M.-S., and van Leer, B., "Inviscid Flux-Splitting Algorithms for Real Gases with Non-Equilibrium Chemistry," *Journal of Computational Physics*, No. 90, 1990, pp. 371–395.

[14]Swanson, R. C., and Turkel, E., "Aspects of a High-Resolution Scheme for the Navier–Stokes Equations," AIAA 93-2272, June 1993.

[15]Martinelli, L., and Jameson, A., "Validation of a Multigrid Method for the Reynolds Averaged Equations," AIAA Paper 88-0414, 1988.

[16]Kunz, R. F., and Lakshminarayana, B., "Explicit Navier–Stokes Computation of Cascade Flows Using the k-ϵ Turbulence Model," *AIAA Journal*, Vol. 30, No. 1, 1992, pp. 13–22.

[17]Gerlinger, P., Algermissen, J., and Brüggemann, D., "Simulation of Turbulent Slot Injection of Different Gases into a Supersonic Air Stream," AIAA Paper 94-2247, June 1994.

[18]Burrows, M. C., and Kurkov, A. P., "Supersonic Combustion of Hydrogen in a Vitiated Air Stream Using Stepped-Wall Injection," AIAA Paper 71-721, June 1971.

[19]Mani, M., Tiwari, S. N., and Drummond, J. P., "Investigation of Two-Dimensional Chemically Reacting and Radiating Supersonic Channel Flows," AIAA Paper 88-0462, Jan. 1988

[20]Yee, H. C., and Shinn, J. L., "Semi-Implicit and Fully Implicit Shock-Capturing Methods for Nonequilibrium Flows," *AIAA Journal*, Vol. 27, No. 3, 1989, pp. 299–307.

[21]Yee, H. C., and Shinn, J. L., "Extension of a Semi-Implicit Shock-Capturing Algorithm for 3-D Fully Coupled, Chemically Reacting Flows in Generalized Coordinates," AIAA Paper 87-1577, June 1987.

[22]Hsu, A. T., Tsai, Y.-L. P., and Raju, M. S., "A PDF Approach for Compressible Turbulent Reacting Flows," AIAA Paper 93-0087, Jan. 1993.